Materials Characterization 135 (2018) 76–83

Contents lists available at ScienceDirect

Materials Characterization

journal homepage: www.elsevier.com/locate/matchar

Microstructure and mechanical properties of extruded Mg-Gd-Y-Zn-Zr alloys filled with intragranular LPSO phases

Xiaojie Zhou[a,b], Chuming Liu[b,c], Yonghao Gao[a,b,*], Shunong Jiang[d], Wenhui Liu[c], Liwei Lu[c]

[a] State Key Laboratory for Powder Metallurgy, Central South University, Changsha 410083, China
[b] School of Materials Science and Engineering, Central South University, Changsha 410083, China
[c] School of Materials Science and Engineering, Hunan University of Science and Technology, Xiangtan 411201, China
[d] School of Civil Engineering, Central South University, Changsha 410083, China

ARTICLE INFO

Keywords:
Magnesium alloy
LPSO
Dynamic recrystallization
EBSD
Mechanical property

ABSTRACT

A comparison has been made on the dynamic recrystallization (DRX), texture, and mechanical properties of the Mg-5.5Gd-4.4Y-1.1Zn-0.5Zr (wt%) alloys extruded with different ratios (ER, 36 and 7.1). Intragranular long-period stacking ordered (LPSO) phases strongly restrict the DRX by restraining the lattice rotation of α-Mg grains and hindering the migration of the boundaries of DRX-ed grains. Extrusion with ER of 36 can widely break the intragranular LPSO phases and create a fully DRX-ed microstructure with a relatively random texture, while the lower ER of 7.1 fails to break the LPSO and leads to a bimodal microstructure with a strong basal fiber texture. Finer DRX-ed grains and smaller LPSO phases account for the superior tensile yield strength and elongation of the ER36 alloy. However, the ultimate tensile strength of the ER7.1 alloy catches up because its larger grain size causes an increase in the strain hardening rate.

1. Introduction

Magnesium alloys have attracted increasing attention in the aerospace, automotive, and transportation industries, because of their low density and high specific strength [1]. Particularly, the alloys containing long-period stacking ordered (LPSO) phases have been extensively studied for their excellent mechanical properties and peculiar microstructural characteristics [2–12]. Hot deformation can eliminate the porosities in casting, refine the grains, crush the secondary phases, and eventually improve the mechanical properties [13]. Among the methods for manufacturing large-scale ingots, extrusion was widely utilized because the billets may be subjected to compressive forces only [14]. This kind of stress condition can overcome the shortcoming of low formability of Mg alloys. A high-performance $Mg_{97}Zn_1Y_2$ (at.%) alloy was developed by rapidly solidified powder metallurgy (RS P/M) processing and extrusion, which exhibits the tensile yield strength of 610 MPa and elongation of 5% [2]. Homma et al. [3] fabricated an extraordinary high-strength Mg-1.8Gd-1.8Y-0.7Zn-0.2Zr (at%) alloy by extrusion. Moreover, the effects of alloy composition [4], volume fraction of LPSO phases [5], and annealing treatment [6] on the microstructure and mechanical properties of the extruded LPSO-containing Mg alloys were also studied. In the majority of the above researches, extrusion with constant parameters was merely applied as a deformation method to trigger dynamic recrystallization (DRX) and induce grain refinement. There are, however, few studies on the influence of extrusion ratio (ER) on the microstructure and mechanical properties of the Mg alloys with LPSO phases.

In addition, it is noteworthy that numerous thin-platelet LPSO phases may appear in the grain interior of the direct chill (DC) casted Mg-6.9Gd-3.2Y-1.5Zn-0.5Zr (wt%) alloy and these phases were proved to restrict DRX during compression [11,12]. However, the evolution of these phases and their effects on DRX during the deformation with different accumulated strain remain unclear. In this paper, numerous thin-platelet LPSO phases were also obtained in the DC casted Mg-5.5Gd-4.4Y-1.1Zn-0.5Zr (wt%) alloy after homogenization (Fig. 1a). A comparison has been made on the DRX, texture, evolution of LPSO phases, and mechanical properties of these peculiar alloys which were extruded with different ratios.

2. Material and Methods

The as-cast ingot with a size of Φ 430 mm × 2000 mm was produced using the direct chill casting technology. Chippings with a weight of ~5 g were derived from the ingot by drilling for the composition detection. The composition was examined to be Mg-5.5Gd-4.4Y-1.1Zn-0.5Zr (wt%) by an inductively coupled plasma (ICP, SPECTRO BLUE

* Corresponding author at: State Key Laboratory for Powder Metallurgy, Central South University, Changsha 410083, China.
E-mail addresses: gaoyonghao@csu.edu.cn (Y. Gao), shnjiang@csu.edu.cn (S. Jiang), lwh@hnust.edu.cn (W. Liu).

https://doi.org/10.1016/j.matchar.2017.11.027
Received 15 August 2017; Received in revised form 2 November 2017; Accepted 12 November 2017
Available online 13 November 2017

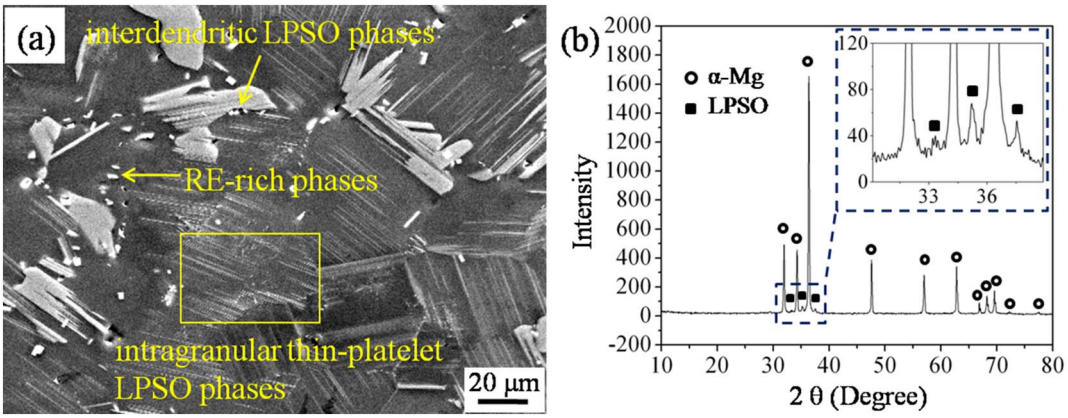

Fig. 1. (a) SEM image and (b) XRD pattern of the as-homogenized Mg-5.5Gd-4.4Y-1.1Zn-0.5Zr alloy.

SOP) analyzer, with the incident frequency of 27 MHZ and power of 1400 W. After homogenization at 783 K for 36 h in a resistance furnace followed by air-cooling, cylindrical billets with the diameter of Φ 390 mm and Φ 115 mm were machined from the center of the ingot. After being held at 673 K (the extrusion temperature) for 1 h, they were extruded to Φ 150 mm and Φ 20 mm in the extrusion container of Φ 400 mm and Φ 120 mm respectively (designated as ER7.1 and ER36 alloy hereafter), with the die half angle of 30°. Considering that these two billets possess different initial diameters, the ram speed was set as ~3 mm s^{-1} and ~0.5 mm s^{-1} respectively for a similar average metal flow rate $\dot{\bar{\varepsilon}}$ ~0.05 s^{-1} (refer to [15]), so as to minimize the effect caused by the size difference. Billets were quenched into water immediately after extrusion.

Microstructure and mechanical properties were studied on the samples derived from the center of the ingots. Tensile tests were conducted on an Instron 3369 tester with the crosshead speed of 1 mm min^{-1}, at room temperature. The tensile axis was parallel to the extrusion direction (ED). More than three specimens, with a gage length of 25 mm and a diameter of 5 mm, were tested to ensure the reliability of the results. Phase morphology and fracture features were characterized by an FEI Sirion200 field-emission scanning electron microscopy (SEM, operated at 20 kV, in secondary electron mode). The constituent phases were identified by the D/Max 2500 X-ray diffraction (XRD) with a Cu Kα radiation, in the 2θ diffraction angle range of 10–80°, at the scanning speed of 8° min^{-1}. Bright-field (BF) images were obtained using an FEI Titan G2 60–300 transmission electron microscope (TEM, operated at 200 kV). Electron back-scatter diffraction (EBSD) was conducted on the HELIOS Nanolab 600i SEM equipped with an HKL EBSD system. The scans were performed using a step size of 0.2 μm. Specimens for TEM and EBSD examinations were twin-jet electron-polished at 233 K and 0.01 A, using a solution of 15 ml perchloric acid and 285 ml ethyl alcohol. EBSD data were used to produce inverse pole figure (IPF) measurements, with high-angle grain boundaries (HAGBs, > 15° misorientation) indicated as black lines and low-angle grain boundaries (LAGBs, > 2° misorientation) as white lines. Grain orientation spread (GOS) was chosen as the basis to distinguish the DRX-ed and deformed regions. In this paper, the grains with GOS < 2° were considered as the DRX-ed grains.

3. Results

3.1. Microstructural Characterization

Fig. 1 shows the SEM image and XRD pattern of the as-homogenized alloy. Apart from the α-Mg matrix, LPSO phases can be detected by the XRD (Fig. 1b). Interdendritic LPSO phases invade the α-Mg grain boundaries and numerous thin-platelet LPSO phases appear inside the α-Mg grains (Fig. 1a). This phenomenon is similar to what was reported in the Mg-6.9Gd-3.2Y-1.5Zn-0.5Zr (wt%) alloy [11,12]. Moreover, some cubic phases form around the grain boundaries. They should be the RE-enriched phases which were widely found in the RE-containing alloys [16,17]. XRD fails to detect them due to their small quantity.

Fig. 2a and b present the IPF maps observed on the transverse sections of the extruded bars, where colors designate the crystal orientation with respect to the sample normal (i.e., ED) as shown in the color triangle (Fig. 2c). The black regions in the IPF maps mainly represent the LPSO phases, since the EBSD system failed to recognize the LPSO phases due to the negligible confidence index (CI) caused by a lack of corresponding phase parameters. Fig. 2d and e show the optical micrographs observed on the longitudinal sections of the extruded bars. In the ER7.1 alloy (Fig. 2a and d), extensive coarse deformed grains filled with thin-platelet LPSO phases still remain. DRX-ed grains appear near the initial grain boundaries, especially around the interdendritic phases. The average size of the DRX-ed grains is about 4.5 μm, with the DRX regions occupying ~36% of the α-Mg regions. According to the color triangle shown in Fig. 2c, it can be detected that the $\langle 01\bar{1}0\rangle$ axis of most deformed grains tends to be parallel with ED, while the DRX-ed grains show more random orientation. Moreover, numerous LAGBs appear in the deformed grains as indicated by the white lines in Fig. 2a. In the ER36 alloy (Fig. 2b and e), however, DRX occurs adequately. Equiaxed DRX-ed grains with an average size of ~2.2 μm occupy 83% of the α-Mg regions, and interdendritic LPSO phases tend to align along ED (Fig. 2e).

Fig. 3 shows the local misorientation maps of the extruded alloys. According to the color bar, the color change from blue through green to red indicates the increase of local residual plastic strain concentration, which represents the enlarged level of dislocation density [18–20]. The zones near the boundaries of deformed grains are mainly presented in green and yellow while the DRX-ed grains are presented in blue, indicating that the dislocation density in the deformed grains is higher than that in the DRX-ed ones.

The EBSD-derived pole figures of the as-extruded alloys are shown in Fig. 4. The ER7.1 alloy exhibits the typical basal fiber texture with (0002) plane and $\langle 01\bar{1}0\rangle$ axis parallel to ED, while the ER36 alloy shows a much weaker texture and more random crystal orientation. The maximum value of pole intensity of the ER36 and ER7.1 alloy is 4.3 and 10.6, respectively. In order to further investigate the texture characteristics, a detailed analysis of the deformed and DRX-ed regions in the ER7.1 alloy is shown in Fig. 5. Compared with the whole alloy, a stronger basal fiber texture with an intensity of 16.0 can be observed in the deformed regions. However, in the DRX-ed regions, although the basal fiber texture dominates, its intensity becomes much weaker (2.7) and another texture component of $\langle 0001\rangle$ //ED can be detected.

The morphology of secondary phases is shown in Fig. 6. Smaller but denser interdendritic fiber-like phases are observed in the alloy with the higher ER (compare Fig. 6a with Fig. 6d). Kink bands of the fiber-like